Stability of Trimeric OmpF Porin: The Contributions of the Latching Loop L2[†]

Prashant S. Phale,[‡] Ansgar Philippsen,[§] Thomas Kiefhaber,[||] Ralf Koebnik,[‡] Vrishali P. Phale,[‡] Tilman Schirmer,[§] and Jurg P. Rosenbusch*,[‡]

Divisions of Microbiology, Structural Biology and Biophysical Chemistry, Biozentrum, University of Basel, CH-4056 Basel, Switzerland

Received May 22, 1998; Revised Manuscript Received September 4, 1998

ABSTRACT: The channel-forming protein OmpF porin from *Escherichia coli* spans the bacterial outer membrane. Each of the three monomers comprises a hollow, 16-stranded β-barrel. These are associated to homotrimers which are unusually stable, due mostly to hydrophobic interactions between the β-barrels. In addition, a loop, L2 connects one subunit to its neighbor by latching into its channel. Residue E71 on loop 2 is integrated into an ionic network and forms salt bridges and hydrogen bonds with R100 and R132 on the channel wall in the adjacent subunit. To examine these contributions quantitatively, six single-site, two double, and one deletion mutant were constructed on the basis of the atomic coordinates of the protein. Differential scanning calorimetric analysis showed that the salt-bridge, E71-R100, contributes significantly to trimer stability: the substitution E71Q causes a decrease of the transition temperature from 72 to 48 °C, with ΔH_{cal} diminishing from 430 to 201 kcal mol^{-1}. A nearby substitution in the loop, D74N, has lesser effects on thermal stability, while the deletion in L2 (Δ69−77) has an effect comparable to that of E71Q. X-ray structure analysis to 3.0 Å resolution revealed only local structural differences in the mutants except for the substitution R100A, where another residue, R132, is found to fill the gap left by the truncated side chain of A100. Functional assays in planar lipid bilayers show significantly increased cation selectivities if the charge distribution was affected.

Porins are proteins forming water-filled, voltage-gated channels across outer membranes of Gram-negative bacteria, such as *Escherichia coli* (*1*). While outer membranes serve as barriers protecting the cytoplasmic membrane from noxious agents such as bile salts, proteases, lipases, and toxins, the passage of nutrients and metabolites is secured by porin channels, which facilitate diffusion of polar solutes of <400 Da. The porins are homotrimers (Figure 1) formed by three hollow β-barrels consisting of 16 antiparallel β-strands each (*2*−*4*). The trimers are extremely stable in that they withstand heat, chaotropic salts, organic solvents, detergents, a wide pH range, and exposure to proteolysis (*5*−*8*). A closely packed hydrophobic core is formed in the trimer (*3*) and is assisted by apolar contacts between the constriction loop L3 and the barrel wall (Figure 1). A hydrogen-bonding network linking L3 to the wall, and steric interactions between the tip of L3 and the β-barrel (*9*) are also involved. This latter motif is conserved in the three-dimensional structure in the specific porins we investigated (*10*, *11*), suggesting that it functions as brace or girder in the near-cylindrical β-barrel. In addition to the extended apolar contact areas, loop L2 reaches over to the neighboring subunit, forming polar and ionic intersubunit interactions. Involved in this is the glutamyl residue 71 (E71) which forms four H bonds with the guanidinium groups of R100 and R132 across the interface (Figures 1C and 2B). D74 is forming intraloop H bonds (Figure 2A) and is thought to contribute to the internal stabilization of the loop.

In this study, we present a quantitative evaluation of the contributions to trimer stability of the polar interactions just outlined, which concern the latching loop L2 and the neighboring monomer. The changes in function of the mutants are correlated to the structural alterations in these mutants.

MATERIALS AND METHODS

Porin Mutants, Functional Assays, and X-ray Analysis. Porin mutants were designed on the basis of the atomic coordinates of porin (*3*) and constructed by site-directed mutagenesis as described previously (*12*). Overexpressed proteins were purified according to established protocols (*9*), which involves the detergents SDS for extraction and octyl-POE for purification. Employing the planar lipid bilayer technique, single channel ion conductance and zero-current potentials were measured as described (*13*). To secure good reproducibility of the zero-current potential measurements, solutions were well stirred (500 rpm), with a distance between the magnetic bar and the stirrer of 2.5 cm. Ion

[†] This work was supported by grants from the Swiss National Science Foundation to J.P.R. and T.S. and by support from EU-BIOTECH/BBW to J.P.R.

* To whom correspondence should be addressed. E-mail: rosenbusch@ubaclu.unibas.ch.

[‡] Division of Microbiology.

[§] Division of Structural Biology.

[||] Division of Biophysical Chemistry.

[1] Abbreviations: DSC, differential scanning calorimetry; octyl-POE, octylpolyoxyethylene; SDS, sodium dodecyl sulfate; PAGE, polyacrylamide gel electrophoresis.

10.1021/bi981215c CCC: $15.00
Published on Web 10/20/1998

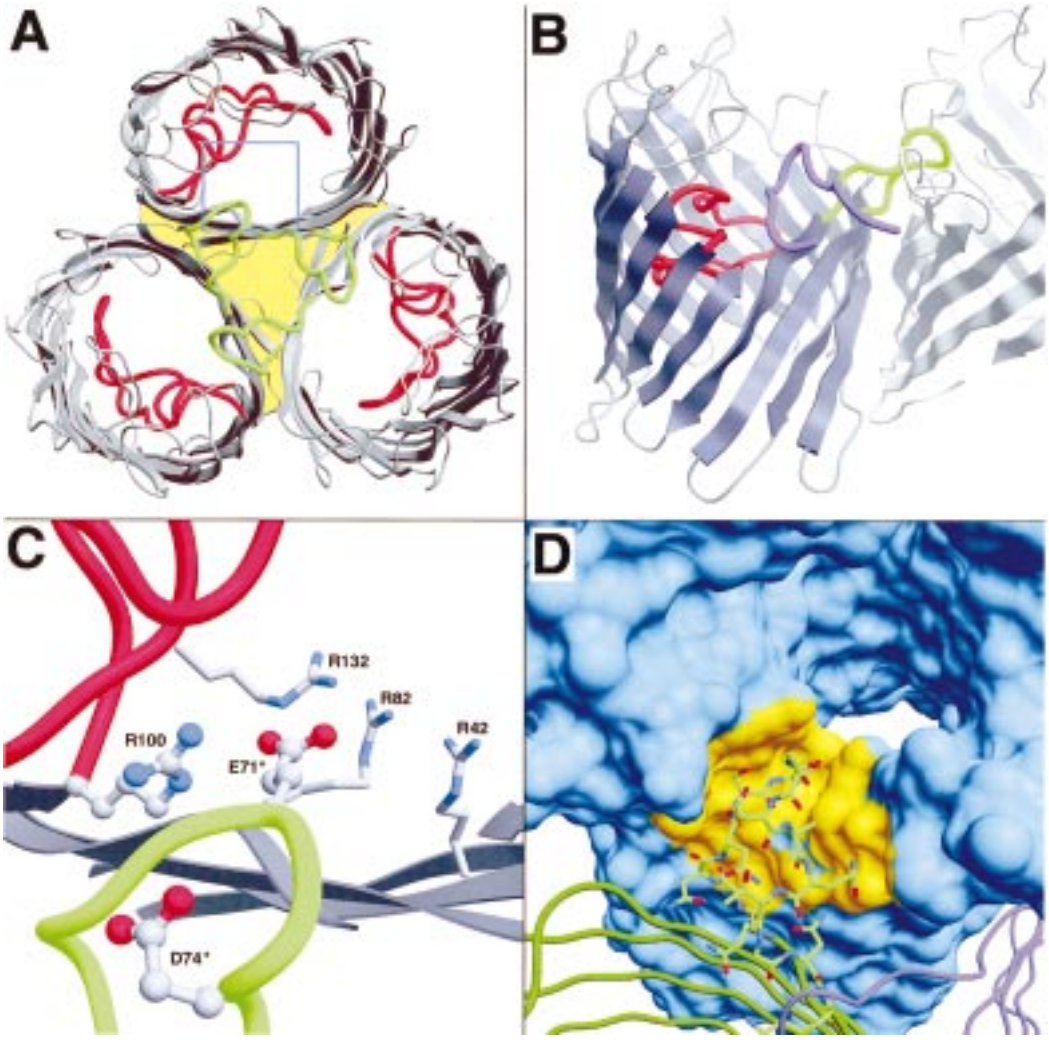

FIGURE 1: The interaction of the latching loop L2 of wild-type OmpF porin with the β-barrel of an adjacent subunit near the constriction site as revealed by the crystal structure (*3*). (A) Top view of the OmpF trimer. It can be seen how loops L2 (green) interact by forming cyclic intersubunit contacts, reaching over into the neighboring subunits. The extended hydrophobic contact between the β-barrels is shaded in yellow. (B) Schematic representation of an OmpF-porin as viewed from the (vertical) 3-fold symmetry axis. The monomer which would face the viewer has been clipped off and only its loop L2 (purple) is seen. This loop is inserted into a gap in the barrel wall of the left monomer, originating from loop L3 (red) folding away into the channel. Loop L2 (green) from the left monomer latches outward to contact the right monomer in an identical manner. (C) Close-up view of the interface between between L2 and the adjacent subunit (framed in panel A). The three residues investigated in this study (R100, E71*, and D74*; the asterisks denote residues from the adjacent subunit) and the residues of the arginine cluster at the pore constriction (R42, R82, and R132) are shown in full. (D) View onto the contact region between loop L2 and the adjacent monomer (similar orientation as in panel C). The surface of one monomer is shown in blue. The backbones of the other two monomers are depicted in green and purple. The area of the monomeric surface that is within 4 Å of the residues from the adjacent loop L2 (green stick model, residues 66−80) amounts to 575 Å^2 and is shown in yellow. The figure was produced with DINO (*31*), the surface was generated with MSMS (*32*).

selectivities (P_{Na}/P_{Cl}) were derived according to Hodgkin and Katz (*14*). Mutant porins inserted into bilayers as efficiently as wild-type protein, resulting in low noise channel recordings. Crystallization was carried out as described for wild-type protein (*15*). The methods and programs applied for crystal structure analyses of the wild-type protein were those described previously (*9*). Crystals of mutant proteins (space group *P*321; typical size, 0.3 × 0.3 × 0.3 mm^3) were isomorphous to wild-type porin, irrespective of whether SDS was used in the purification (*9*) or not (*15*). The variance in the cell constants was <1% and they were set to wild-type values ($a = b = 118.5$ Å; $c = 52.7$ Å) for all mutants. Structures were determined by the difference Fourier technique based on the wild-type model (*3*). For the R_{free}-calculations, the same test set as for the wild-type porin was used. Refinement was performed with the program REFMAC from the CCP4 suite (*16*) using the MLKF target.

Thermal Stability of Trimers. SDS−PAGE was performed to determine the temperature of trimer dissociation (T_d) of the various porin mutants. Protein samples (5 μg) containing SDS and β-mercaptoethanol at final concentrations of 1 and 2.5%, respectively, were incubated for 10 min at various temperatures (40−100 °C, in steps of 5 °C). Shifts in electrophoretic mobilities, due to the conversion of trimers into monomers (*5*), was monitored by PAGE (12%) in SDS. Changes in the specific heat capacity of protein solutions were determined by differential scanning calorimetry (DSC) on a MC-2 Scanning Calorimeter (MicroCal, Northampton, MA 01060). Mutant porin proteins (final concentration 1.0 mg/mL, i.e., 9 μM trimers) were dissolved in 25 mM

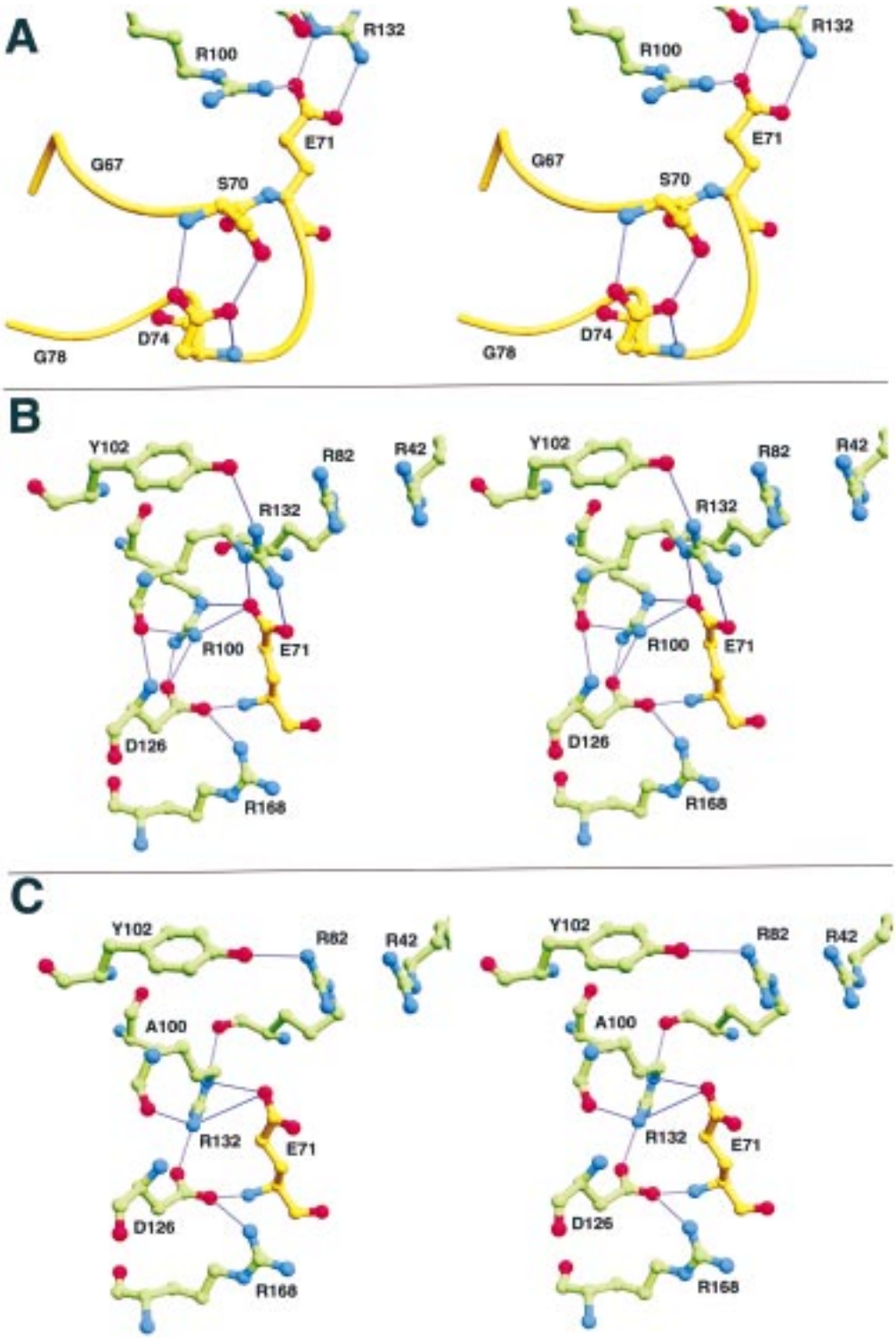

FIGURE 2: Stereoscopic picture of the structure of L2 (yellow) with key residues from the neighboring subunit (in green). (A) D74 is H bonded to the main-chain amide and the side-chain hydroxyl of S70. H-bonds are shown by thin lines. For clarity, the contacts of E71 with R100 and R132 of the neighboring subunit are shown. (B) Detailed stereoscopic view of the subunit-subunit interface around E71 in wild-type OmpF. The arginine cluster (R42, R82, and R132) that lines the channel can be seen in the upper half of the figure. E71 (yellow) is part of an ionic H-bonded network, together with R100, D126, and R132. Intersubunit hydrogen bond distances are as follows: $E71O_{\epsilon 1}-R132N_{\eta 2}$, 2.9 Å; $E71O_{\epsilon 2}-R132N_{\epsilon}$, 2.6 Å; $E71O_{\epsilon 2}-R100N_{\eta 2}$, 3.1 Å; $E71O_{\epsilon 2}-R100N_{\epsilon}$, 3.5 Å; $E71N-D126\ O_{\delta 2}$, 2.9 Å. (C) Structure of the interface mutant R100A in the same representation as in panel B. R132 has changed its conformation and has adopted the position that is taken by R100 in the wild-type porin. Intersubunit contacts are as follows: $E71O_{\epsilon 2}-R132N_{\eta 1}$, 4.1 Å (probably no longer forming a strong interaction); $E71O_{\epsilon 2}-R132N_{\epsilon}$, 3.7 Å; $E71N-D168O_{\delta 2}$, 3.1 Å. The figure was produced with DINO (*31*).

phosphate (NaP_i) buffer (pH 7.4) containing 1% SDS. Scans were performed at a rate of 45 °C/h. Slower scanning rates (10 °C/h, 20 °C/h) yielded same results. The values of temperature and excess heat capacity were recorded every 15 s. Measurements of all samples were preceded by baseline scans with buffer only in the sample compartment. Each measurement was performed three times. The excess heat capacity curves were analyzed by using the software Mi-

Table 1: Trimer Thermal Stability and Thermodynamic Properties of Wild-Type and Various Loop L2 Mutants of OmpF

		DSC				derived values		
protein	SDS−PAGE, T_d[a] (°C)	T_m[b] (°C)	$\Delta T_{1/2}$ (°C)	ΔH_{cal} (kcal mol^{-1})	$\Delta S_{(Tm)}$ (kcal mol^{-1} K^{-1})	$\Delta H_{(25°C)}$ (kcal mol^{-1})	$\Delta S_{(25°C)}$ (kcal mol^{-1} K^{-1})	$\Delta G_{(25°C)}$ (kcal mol^{-1})
wild-type	70 (75)	72.0	3.7	430	1.2	−54	−0.26	24
E71A	55 (60)	56.6	5.1	268	0.81	−57	−0.22	10
E71Q	50 (50)	47.7	4.8	201	0.63	−32	−0.13	6.6
R100A	60 (65)	60.3	3.1	354	1.1	−9	−0.09	18
R100S	55 (60)	58.2	3.3	324	0.98	−17	−0.11	16
E71A/R100A	55 (60)	55.0	4.6	233	0.71	−76	−0.28	6.7
E71Q/R100S	50 (55)	49.1	4.5	173	0.54	−75	−0.26	3.6
D74A	60 (70)	63.3	3.8	320	0.95	−74	−0.29	14
D74N	60 (70)	65.4	3.9	372	1.1	−44	−0.21	19
ΔL2 (69-77)	45 (55)	43.4	9.5	131	0.41	−58	−0.2	2.5

[a] Temperature of trimer dissociation (T_d) is defined as the temperature at which the monomer band on the SDS−PAGE starts to appear. The temperature values in parentheses indicate the temperature of complete conversion of trimers into monomers. [b] The phase transition as observed by DSC is characterized by the transition temperature (T_m), the width at half-height of the transition ($\Delta T_{1/2}$), and the calorimetric enthalpy of unfolding (ΔH_{cal}). $\Delta H_{(25°C)}$, $\Delta S_{(25°C)}$, and $\Delta G_{(25°C)}$ were derived as described in the Materials and Methods.

croCal-MC-2 (MicroCal, Northampton, MA 01060). The "single 2-state transition with dissociation" model gave the best fits (mean $\chi^2 = 3 \times 10^6$) and was used throughout. The variance in the ΔH_{cal} values was ±5%.

Extrapolation of ΔH_{cal} to a reference temperature T was performed according to (*17*−*19*):

$$\Delta H_{(T)} = \Delta H_{cal} + \Delta C_p(T - T_m)$$

Similarly, the entropy and free-energy change at the reference temperature were obtained from the relations

$$\Delta S_{(Tm)} = \Delta H_{cal}/T_m$$

$$\Delta S_{(T)} = \Delta S_{(Tm)} + \Delta C_p \ln(T/T_m)$$

$$\Delta G_{(T)} = \Delta H_{(T)} - T\Delta S_{(T)}$$

RESULTS

Nine mutants in OmpF porin (Table 1) were examined to assess the contribution of loop L2 to trimer stability. This loop makes extensive polar contacts with the adjacent subunit (Figure 1 and Figure 2). Upon oligomerization, a large surface area (575 Å^2, Figure 1D) of each loop 2 becomes inaccessible to solvent. Mutants with substitution at position E71, R100, E71/R100, D74, and a deletion mutant ΔL2 (69−77) yielded good expression, inserting as efficiently during growth as wild-type into the outer membrane of *E. coli*.

Thermal Stability of OmpF Mutants. The temperature of trimer dissociation in SDS, T_d, as analyzed by polyacrylamide gel electrophoresis is significantly lower in all mutants investigated (Table 1). The largest effect is observed for the variants which have a change in E71, including the deletion of residues 69−77 in L2 (called ΔL2). Replacement of residue D74 shows only a marginal decrease in T_d. The results for wild-type and mutant E71Q porin are shown in Figure 3A. For comparison, we have also determined T_d of the previously described porin mutants with substitutions in the constriction loop L3 and the L3-barrel interface (*9*). All of them exhibited essentially wild-type behavior (data not shown), with T_d between 65 and 70 °C.

The enthalpies of thermal unfolding, ΔH_{cal}, were measured by DSC (Table 1). Figure 3B shows the excess heat capacity curves for wild-type and three mutant porins. Except for ΔL2, the observed transitions were sharp (see $\Delta T_{1/2}$ in Table 1, Figure 3B). No indication for the occurrence of inter-

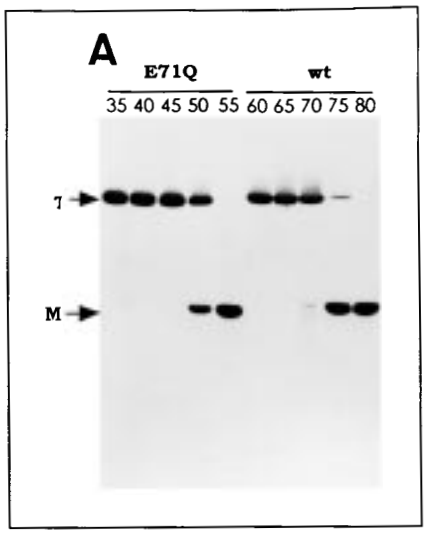

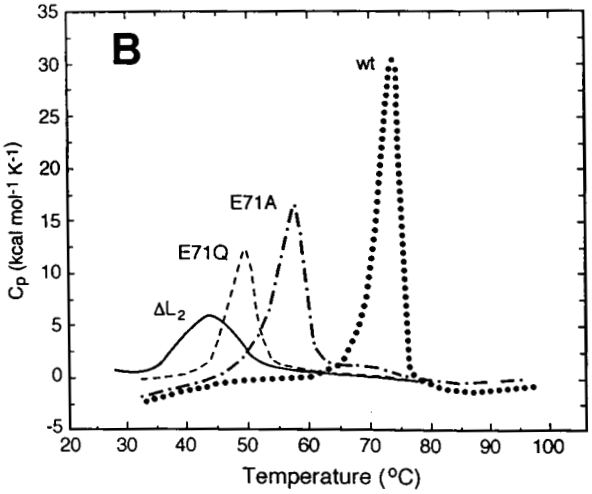

FIGURE 3: Analysis of thermal stability of OmpF variants. (A) SDS−PAGE analysis of E71Q and wild-type (wt) OmpF. The incubation temperatures are indicated at the top of the lanes. T indicates the trimeric protein, M, the denatured monomer; (B) DSC analysis of wild-type OmpF (wt), and mutants ΔL2, E71A and E71Q. The excess heat capacities have been normalized for the monomer concentration.

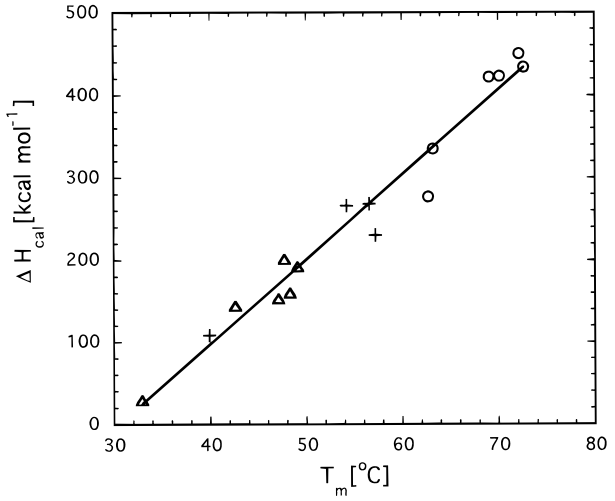

FIGURE 4: Plot of the calorimetric transition enthalpies (ΔH_{cal}, normalized with respect to trimer concentration) versus the transition temperature (T_m) for wild-type porin (circles), mutant E71A (+), and E71Q (triangles). These data were obtained by variation of the pH in the range 5.4−10.4. Additional data are given in Supporting Information.

mediates during the process was seen. All data could be fitted very well (see Supporting Information) to a $N_n \leftrightarrow nD$ model if $n = 3$ was chosen, implying perfect cooperativity among the subunits during unfolding. Rescanning the same sample after slow cooling did not reveal refolded protein.

The observed transition temperatures (T_m) agree well with the T_d values obtained from the SDS−PAGE experiments (Table 1). The enthalpies of unfolding, ΔH_{cal}, are considerably reduced for all of the mutants in comparison to wild-type porin. The largest effect is observed for the deletion mutant ΔL2 and for mutations at position 71. Similar effects are observed for the change in entropy, $\Delta S_{(Tm)}$. The molar heat capacity change upon unfolding ΔC_p was obtained by monitoring the pH-dependent change of ΔH_{cal} and T_m. To cover a large temperature range, all the data obtained for wild-type porin, E71A, and E71Q were taken into account. The corresponding ΔH_{cal} versus T_m plot (Figure 4) shows a linear relationship and gives a ΔC_p of 10.3 ± 0.5 kcal mol^{-1} K^{-1}. The good fit allowed the thermodynamic quantities to be extrapolated to room temperature (Table 1). As judged by the change in free energy, $\Delta G_{(25\ °C)}$, ΔL2 and mutants with replacements at position 71 are least stable, while mutants with substitutions at position 74 or 100 are nearly as stable as the wild-type porin.

Structural Analysis. The structures of five mutants were determined by X-ray analysis. Crystallographic details are given in Table 2. In all cases, only local yet distinct changes in the vicinity of the replaced side chains were observed.

Mutants E71A and E71Q. In both mutant structures, well-defined electron density is seen at the position occupied by the side chain of E71 in the wild-type (Figure 5, panels A−C). This density in the mutants probably represents an anion, as is inferred from the close proximity to the two guanidinium groups of R100 and R132 (3.1 Å each). The magnitude of the electron density and the composition of the mother liquor are consistent with a Cl^- ion. In mutant E71Q, the glutamine side chain is pointing outward and is not interacting with the arginine residues.

Table 2: Crystallographic Statistics of OmpF Mutants

	mutant				
data	E71A	E71Q	D74A	R100A	E71A/R100A
resolution (Å)	3.0	3.0	3.0	3.0	3.0
no. of unique reflections	7459	8612	8162	7958	8336
completeness (%)	85	98	92	93	95
redundancy	2.8	8.6	3.9	1.6	4.3
R_{merge} (%)	10.0	11.6	8.2	9.4	9.4
R (%)	19.3	20.1	19.1	20.0	20.2
R_{free} (%)	28.9	28.6	26.9	29.5	28.6
rms deviation					
bond length (Å)	0.009	0.010	0.010	0.009	0.009
bond angles (Å)	0.036	0.038	0.039	0.034	0.036
mutant−wild-type (Å)	0.21	0.21	0.18	0.20	0.20

Mutants R100A and E71A/R100A. In wild-type porin, R100 is forming ionic interactions with E71* (asterisks denote residues from an adjacent subunit) and D126 (Figure 2B). In R100A, the gap left by the truncated arginine side chain is occupied by R132, which now forms a salt-bridge with D126. The guanidinium group of R132 has moved by 6.6 Å, and as a consequence, the arginine cluster in the pore constriction, consisting of R42, R82, and R132 (*3*, *20*), is perturbed by a water molecule filling the void left by the guanidinium group of R132. The side chains of R42 and R82 have moved slightly toward this water molecule by 0.7 and 0.9 Å, respectively, while the side chain of Y102 has moved away by 0.5 Å (Figure 5D and Figure 2C). E71* is released from the ionic network. Virtually the same structure is observed for the double mutant E71A/R100A with the side chain 71 truncated.

Mutant D74A. In wild-type porin, the carboxylate of D74 interacts with the main-chain amide and the side-chain hydroxyl of S70 at the base of L2 (Figure 2A) thereby tying them together. In the mutant, this interaction is lost and the tip of the loop is less kinked (Figure 5E). Side chains 73 and 74 have moved by 0.8 and 0.6 Å, respectively. No water is observed in the space left by the former aspartyl side chain of residue 74.

Functional Characterization of Mutants. Mutants were characterized functionally in planar lipid bilayers (Table 3). Single channel conductance values are found slightly reduced. Ion selectivities are virtually unchanged except for the R100 mutants which, compared to the wild-type protein, are more cation selective. For most of the mutants, the critical voltage V_c for channel closing was similar to the values obtained for the wild-type protein [+150 mV (*9*, *13*)], except for E71A and E71Q which showed an increase in V_c to 180−200 mV.

DISCUSSION

The high-resolution X-ray structure of OmpF trimers shows extensive and intimate contacts among its three subunits, indicating that the three hollow β-barrel structures stabilize each other mutually (*3*). Indeed, it was observed early that OmpF porin cannot be dissociated without concomitant denaturation of the monomer above 60 °C (*5*) and that its stability is such that the protein is equally unperturbed by harsh detergents [2% SDS at neutral pH (*5*, *7*)], by mild detergents (e.g., octyl-POE), or by chahopic agents (urea, guanidinium salts). Moreover, the trimers of

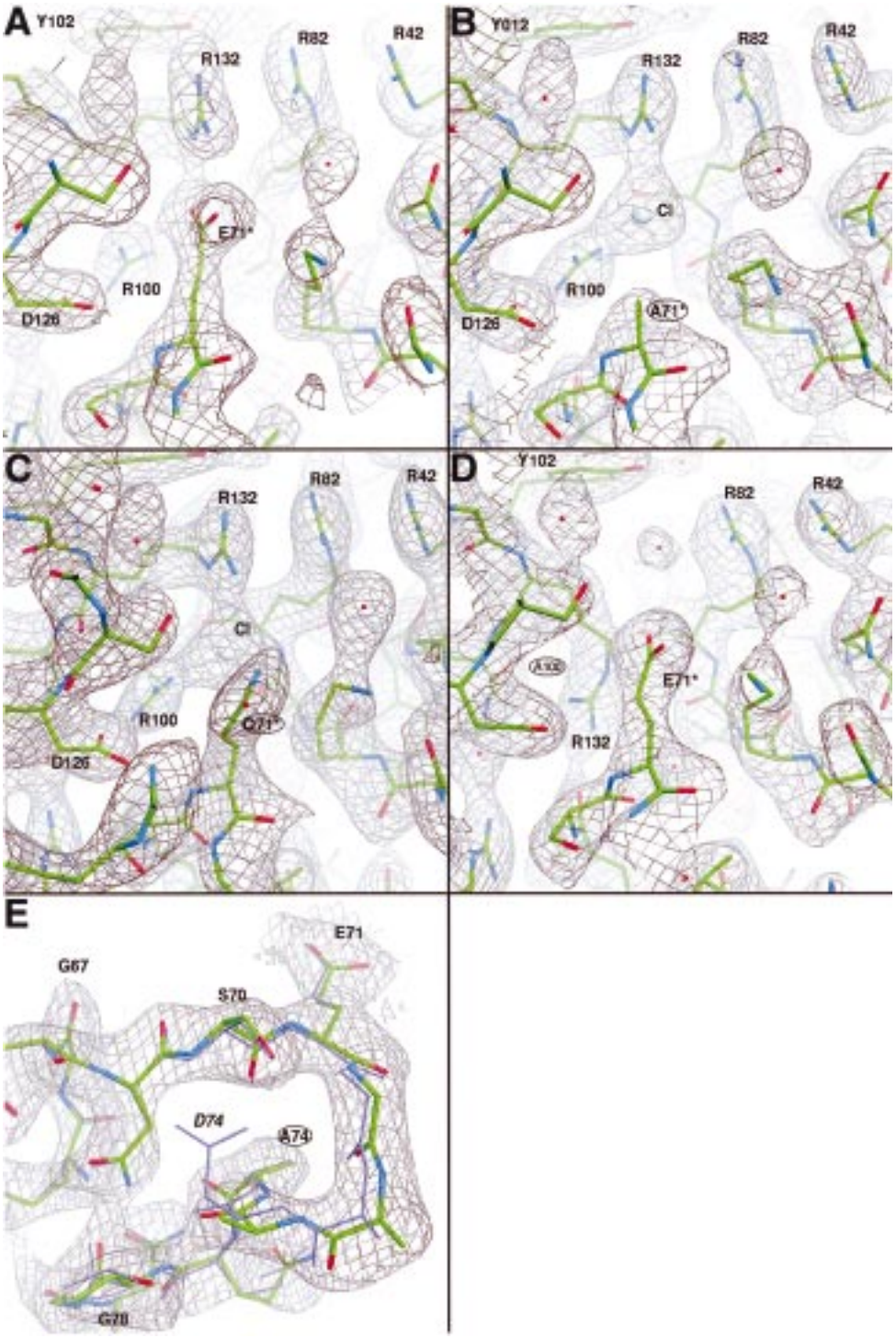

FIGURE 5: Crystal structures of loop L2 with interacting residues in wild-type and mutant OmpF. The refined models are superimposed onto the $2F_o - F_c$ electron density maps (contoured at 1σ). Mutated residues are encircled. (A) OmpF wild-type. (B) Mutant E71A. (C) E71Q. The glutamine side chain of residue 71 can apparently no longer integrate into the hydrogen-bond network (with R100 and R132) as in wild-type OmpF (see panel A and Figure 3) and has shifted its position by 3.1 Å toward the viewer. The position of the former glutamyl group is occupied by a chloride ion (as in E71A, see Panel B), with which Q71 interacts (distance $E71N_{\epsilon 2}-Cl^-$, 3.0 Å); (D) R100A, the mutated residue is in the background; (E) D74A with superimposed model of wild-type OmpF in purple. The figure was produced with DINO (*31*).

porin do not bind SDS (*6*). The stability facilitates crystallization and the ionic detergent appears unlikely to affect key ionic interactions in the crystal (see Materials and Methods). Here, we show that tampering with the subunit interfaces by replacing crucial residues results in distinctively lower temperatures of denaturation. Even at these lower temperatures (e.g., 43 and 48 °C for ΔL2 and E71Q, respectively), folded monomers of OmpF porin were not detected. In contrast, a mutation E66R in phosphoporin (corresponding to position 71 in the OmpF sequence) resulted in folded PhoE monomers at room temperature (*21*), demonstrating the drastic effect of an acidic to a basic substitution at that position.

The transitions to unfolded states, as monitored by DSC, yielded single, asymmetric peaks, without indications for the occurrence of intermediates. The data can be fitted well to

Table 3: Functional Properties of OmpF Mutants

protein	conductance Λ (nS)	ion selectivity P_{Na}/P_{Cl}
wild-type	0.84 ± 0.06 (n = 158)	4.5 ± 0.8 (m = 6)
E71A	0.65 ± 0.02 (n = 80)	4.9 ± 0.4 (m = 4)
E71Q	0.73 ± 0.07 (n = 73)	4.8 ± 0.4 (m = 5)
R100A	0.76 ± 0.02 (n = 203)	6.8 ± 0.3 (m = 5)
R100S	0.74 ± 0.02 (n = 189)	5.7 ± 0.1 (m = 4)
E71A/R100A	0.78 ± 0.02 (n = 153)	6.4 ± 0.46 (m = 3)
E71Q/R100S	0.74 ± 0.02 (n = 191)	5.3 ± 0.02 (m = 3)
D74A	0.82 ± 0.02 (n = 116)	4.6 ± 0.34 (m = 4)
D74N	0.85 ± 0.03 (n = 128)	5.0 ± 0.6 (m = 5)
ΔL2 (69-77)	0.76 ± 0.04 (n = 183)	4.4 ± 0.38 (m = 4)

[a] n, number of single channel conductance steps; m, number of different membranes measured.

a $N_3 \leftrightarrow$ 3D two-state model (*22*). Dissociation to an apparent intermediate state, 3N, has been observed previously in the presence of SDS only at pH values ≤3.5 (*7*). Although, here it was not possible to refold the protein by slow cooling, the measured thermodynamic quantities did not depend on scan rates as was observed with bacteriorhodopsin (*23*). Taking these observations together, the unfolding transition is thus probably reversible and followed by a slow irreversible step (for a discussion, see refs *22* and *24*).

Loop L2 contributes to the OmpF stability both by enthalpic and entropic changes, as seen by the reduction in ΔH_{cal} and $\Delta S(T_m)$ in the various mutants. Extrapolation of these values to room temperature, and calculation of the change in free energy, $\Delta G_{(25\ °C)}$, shows that, in agreement with expectations, wild-type porin is most stable, while the deletion mutant ΔL2 is more labile, followed by the stabilities of the single and double mutants involving E71. Interestingly, the mutant E71Q is less stable if compared to E71A. We suggest that the glutaminyl side chain in mutant E71Q does not find a suitable partner (see the legend to Figure 5C) and therefore adopts an energeticaly less favorable position. The replacement of the other partner in the intersubunit salt-bridge, R100, has a less pronounced effect. This is explained by the observation that R132 swings into the vacated space. Thus, an ionic interaction with E71 is reestablished (Figure 2C), although H bonds are absent and the distance is larger (4.8 Å). In line with the minor structural differences observed (Figure 5E) the thermal stability of the D74 mutants is little affected.

Compared to loop L2, the constriction loop L3 appears to play a less significant role for the structural integrity of porin. The investigated L3 mutants of the OmpF porin, including a deletion mutant lacking five residues, showed thermal stability very similar to that of the wild-type porin. In OmpC-porin, a structural homologue of the OmpF porin, a deletion of eight residues in loop 3 caused a reduction of T_m by 16 °C, as measured by DSC (*25*). This value is small if compared to the temperature shift obtained for mutant ΔL2.

In contrast to soluble proteins, few experimental studies have been reported on the thermodynamics of membrane protein stability which are often complicated by the irreversible nature of the transition (*26*). The specific enthalphic change of wild-type OmpF at the transition temperature is $\Delta H = 4.0$ cal g^{-1}. This is considerably less than observed for soluble proteins such as lysozyme ($\Delta H = 10.0$ cal g^{-1}), but it is of the same order than that obtained for the membrane protein bacteriorhodopsin (*26*). The specific heat capacity ΔC_p for wild-type OmpF was determined to be 0.10 cal g^{-1} K^{-1}. This is a typical value for small soluble proteins, while, for bacteriorhodospin, a value of 0.05 cal g^{-1} K^{-1} was found (*27*). It should be pointed out that these data are not directly comparable, because porin denaturation was measured in the presence of a detergent, while soluble proteins and bacteriorhodopsin (in purple patches) have been measured in aqueous environment. Changes in ΔH_{cal} values observed for the OmpF mutants are similar to those determined for loop deletion mutants of bacteriorhodopsin and for bacterio-opsin (*28*), as well as for the bovine opsin (*29*).

The changes in the functional properties of the mutants appear rather unimpressive at first sight. Thus, in the most pronounced case, the conductance value is decreased by 22%. This is hardly surprising, however, since the mutations are at distances of 10 and 14 Å from the center of the channel lumen for E71* and R100, respectively. Also, ion selectivities are not affected in most mutants including ΔL2 (with two acidic residues, E71 and D74 removed), with the interesting exception of those variants with substitutions at position 100, in which a significant increase in cation selectivity is observed. The X-ray structure of R100A (Figure 2C and Figure 5D) yields the following explanation: the rearrangement of the side chain of R132 results in the loss of one residue in the cluster of basic groups at the channel lining (*3*). The effect for the mutant R100S is less pronounced, probably because the S100 side chain does not allow a perfect fit of R132 into its new position. The increase in cation selectivity is comparable to that seen with single arginine mutations in the constriction site (*13*, *30*), whithout being accompanied by a change in voltage sensitivity. Conversely, substitutions of E71 are silent with respect to ion selectivity, yet they do show significant increase of the critical voltage for channel closing. These observations suggests that certain charged residues which are not situated at the constriction site may have an indirect effect on the functional properties of the channels.

In conclusion, it appears that the latching loop 2 has a significant impact on the stability of the trimeric porin. As the constituents of loop 2 interacting with the residues of the adjacent subunit are separated from the main channel lumen, replacements of ionizable groups have an impact only if the mutations affect the hydrogen-bonding system that serves as relay to the channel lumen, as this perturbs the rather rigid arrangement of the three arginyl groups exposed to the channel.

ACKNOWLEDGMENT

We thank Mr. P. Ganz, Department of Biophysical Chemistry, Biozentrum, for assistance with the DSC experiments.

SUPPORTING INFORMATION AVAILABLE

Determination of ΔC_p by monitoring pH dependent changes in the ΔH_{cal} and T_m for wild-type, E71A, and E71Q mutants of OmpF are presented together with two figures and one table (6 pages). Ordering information is given on any current masthead page.

REFERENCES

1. Nikaido, H. (1992) *Mol. Microbiol. 6*, 435−442.

2. Weiss, M. S., Abele, U., Weckesser, J., Welte, W., Schiltz, E., and Schulz, G. E. (1991) *Science 254*, 1627−1630.
3. Cowan, S. W., Schirmer, T., Rummel, G., Steiert, M., Ghosh, R., Pauptit, R. A., Jansonius, J. N., and Rosenbusch, J. P. (1992) *Nature 358*, 727−733.
4. Schirmer, T. (1998) *J. Struct. Biol. 121*, 101−109.
5. Rosenbusch, J. P. (1974) *J. Biol. Chem. 249*, 8019−8029.
6. Rosenbusch, J. P., and Müller, R. (1977) in *Solubilization of Lipo-protein Complexes* (Peeters, H., and Massue, J. P., Eds.) pp 59−68, European Press, Ghent).
7. Schindler, M., and Rosenbusch, J. P. (1984) *FEBS. Lett. 173*, 85−89.
8. Schenkman, S., Tsugita, A., Schwartz, M., and Rosenbusch, J. P. (1984) *J. Biol. Chem. 259*, 7570−7576.
9. Phale, P. S., Schirmer, T., Prilipov, A., Lou, K.-L., Hardmeyer, A., and Rosenbusch, J. P. (1997) *Proc. Natl. Acad. Sci. U.S.A. 94*, 6741−6745.
10. Schirmer, T., Keller, T. A., Wang, Y.-F., and Rosenbusch, J. P. (1995) *Science 264*, 914−916.
11. Rosenbusch, J. P. (1996) *Handbook of Biological Physics: Transport Processes in Eukaryotic and Prokaryotic Organisms* (Konings, W. N., Kaback, H. R., and Lolkema, J. S., Eds.) Vol. 2, pp 599−614.
12. Prilipov, A., Phale, P. S., Van Gelder, P., Rosenbusch, J. P., and Koebnik, R. (1998) *FEMS Microbiol. Lett. 163*, 65−72.
13. Saint, N., Lou, K.-L., Widmer, C., Luckey, M., Lou, K.-L., Schirmer, T., and Rosenbusch, J. P. (1996) *J. Biol. Chem. 271*, 20676−20680.
14. Hodgkin, A. L., and Katz, B. (1949) *J. Physiol. (London) 108*, 37−77.
15. Pauptit, R. A., Zhang, H., Rummel, G., Schirmer, T., Jansonius, J. N., and Rosenbusch, J. P. (1991) *J. Mol. Biol. 218*, 505−507.
16. Collaborative computational project no. 4 (1994) *Acta Crystallogr., Sect. D 50*, 760−763.
17. Kiefhaber, T., Schmid, F. X., Renner, M., and Hinz, H.-J. (1990) *Biochemistry 29*, 8250−8257.
18. Privalov, P. L., and Gill, S. J. (1988) *Adv. Protein Chem. 39*, 191−234.
19. Schellman, J. A. (1987) *Annu. Rev. Biophys. Biophys. Chem. 16*, 115−137.
20. Karshikoff, A., Spassov, V., Cowan, S. A., Ladenstein, R., and Schirmer, T. (1994) *J. Mol. Biol. 240*, 372−384.
21. Van Gelder, P., and Tommassen, J. (1996) *J. Bacteriol. 178*, 5320−5322.
22. Manly, S., Matthews, K., and Sturtevant, J. (1985) *Biochemistry 24*, 3842−3846.
23. Azuaga, A. I., Sepulcre, F., Padros, E., and Mateo, P. L. (1996) *Biochemistry 35*, 16328−16335.
24. Sturtevant, J. M. (1987) *Annu. Rev. Phys. Chem. 38*, 463−488.
25. Rocque, W. J., and McGroarty, E. J. (1990) *Biochemistry 29*, 5344−5351.
26. Stowell, M. H. B., and Rees, D. C. (1995) *Adv. Protein Chem. 46*, 279−311.
27. Brouillette, C. G., Muccio, D. D., and Finney, T. K. (1987) *Biochemistry 26*, 7431−7438.
28. Kahn, T. W., Sturtevant, J. M., and Engelman, D. M. (1992) *Biochemistry 31*, 8829−8839.
29. Miljanich, G. P., Brown, M. F., Mabrey-Gaud, S., Dratz, E. A., and Sturtevant, J. M. (1985) *J. Membr. Biol. 85*, 79−86.
30. Lou, K.-L., Saint, N., Prilipov, A., Rummel, G., Benson, S. A., Rosenbusch, J. P., and Schirmer, T. (1996) *J. Biol. Chem. 271*, 20669−20675.
31. Philippsen, A. (1998) http://www.biozentrum.unibas.ch/~xray/dino/ (accessed February 1998).
32. Sanner, M. F., Spehner, J.-C., and Olson, A. J. (1996) *Biopolymers 38*, 305−320.

BI981215C